2016 23rd International Conference on Pattern Recognition (ICPR)
Cancún Center, Cancún, México, December 4-8, 2016

Separating Reflection Components in Images under Multispectral and Multidirectional Light Sources

Naoto Kobayashi Takahiro Okabe
Department of Artificial Intelligence
Kyushu Institute of Technology
680-4 Kawazu, Iizuka, Fukuoka 820-8502, Japan
Email: okabe@ai.kyutech.ac.jp

***Abstract*—The appearance of an object depends on the color as well as the direction of a light source illuminating the object. The progress of LEDs enables us to capture the images of an object under multispectral and multidirectional light sources. Separating diffuse and specular reflection components in those images is important for preprocessing of various computer vision techniques such as photometric stereo, material editing, and relighting. In this paper, we propose a robust method for separating reflection components in a set of images of an object taken under multispectral and multidirectional light sources. We consider the set of images as the 3D data whose axes are the pixel, the light source color, and the light source direction, and then show the inherent structures of the 3D data: the rank 2 structure derived from the dichromatic reflection model, the rank 3 structure derived from the Lambert model, and the sparseness of specular reflection components. Based on those structures, our proposed method separates diffuse and specular reflection components by combining sparse NMF and SVD with missing data. We conducted a number of experiments by using both synthetic and real images, and show that our method works better than some of the state-of-the-art techniques.**

I. Introduction

The appearance of an object depends not only on the object itself but also on the light source illuminating the object. In particular, it depends on the color, *i.e.* spectral intensity as well as the direction of the light source. Conventionally, the dependencies on lighting color and lighting direction are often studied in separate fields; color analysis (or multispectral imaging) studies images under multispectral light sources whereas shading analysis studies images under multidirectional light sources.

Recently, the progress of light-emitting diodes (LEDs) enables us to capture a set of images of an object under multispectral and multidirectional light sources by using the multi/hyper-spectral light stages [1], [5], [6] which extend the setup of Debevec *et al.* [3] as shown in Fig. 1. It is reported that integrating color analysis and shading analysis by using images under multispectral and mutidirectional light sources is effective for raw material classification [5], bidirectional texture function (BTF) classification [8], and surface reflectance and normal recovery [6].

In general, the reflected light observed on an object surface consists of a diffuse reflection component and a specular reflection component. Separating those reflection components is important for preprocessing of various computer vision techniques such as photometric stereo [15], image-based material editing [9], and relighting [4].

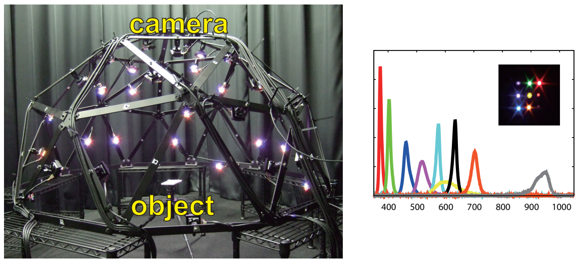

Fig. 1. Our multispectral light stage termed Kyutech Light Stage I [6]. It consists of LED clusters, each of which has LEDs with different spectral intensities.

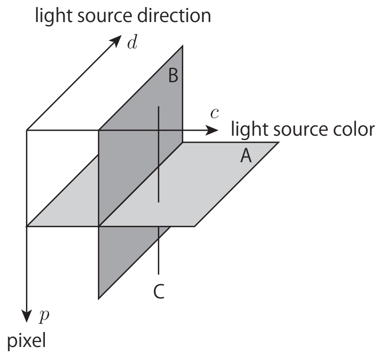

Fig. 2. A set of images of an object captured from a fixed viewpoint but under multispectral and multidirectional light sources are represented as the 3D data whose axes are the pixel p, the light source color c, and the light source direction d.

In this paper, we propose a robust method for separating reflection components in images taken under multispectral and multidirectional light sources. Such a problem is challenging as discussed in more detail in Section II. First, the color-based approach [11] does not work well because the spectral intensities of LEDs are often narrow-band, and then the color of a specular reflection component is almost the same as that of a diffuse reflection component. Second, the approach based on the low-rankness of diffuse reflection components [12] assumes that the light source color is not variable but fixed.

Accordingly, we consider the images of an object captured from a fixed viewpoint but under multispectral and multidirectional light sources as the 3D data whose axes are the pixel p, the light source color c, and the light source direction d as illustrated in Fig. 2. Then, we reveal the inherent structures of

978-1-5090-4846-5/16/$31.00 ©2016 IEEE

the 3D data: the rank 2 structure of pixel values on the slice A in Fig. 2 derived from the dichromatic reflection model [11], the rank 3 structure of diffuse reflection components on the slice B derived from the Lambert model, and the sparseness of specular reflection components. Based on those structures, our proposed method separates diffuse and specular reflection components by combining sparse NMF [10] and SVD with missing data [13].

To confirm the effectiveness of our proposed method, we conducted a number of experiments by using both synthetic and real images. The experimental results show that taking all of the inherent structures of the 3D data into consideration is effective for robustly separating reflection components and that our method works better than some of the state-of-the-art methods based on color [2] and low-rankness [16].

The main contribution of this paper is threefold. First, we address a novel problem of separating reflection components in images under multispectral and multidirectional light sources. Second, we consider those images as the 3D data, and reveal its inherent structure. Third, based on the structure of the 3D data, we propose a robust method for separating diffuse and specular reflection components.

II. Related Work

Existing methods can be classified into three approaches: (i) the color-based approach, (ii) the approach based on the low-rankness of diffuse reflection components, and (iii) the polarization-based approach. In this section, we briefly explain the point of each approach, and then discuss the limitations of those approaches when they are used for separating reflection components in images under multispectral and multidirectional light sources.

The first approach based on color makes use of the difference between the colors of a specular reflection component and a diffuse reflection component. According to the dichromatic reflection model [11], the former is the same as the light source color whereas the latter depends on the spectral reflectance of a surface. The color-based approach has an advantage that it can be applied even to a single image, *i.e.* the column C in Fig. 2.

Unfortunately, however, the color-based approach does not necessarily work well for images taken under LEDs. This is because the spectral intensities of LEDs are often narrow-band. It is almost impossible to distinguish the color of a specular reflection component from that of a diffuse reflection component in a single image taken under a narrow-band light source. In addition, when the color-based approach is used independently for each image, we cannot capture the inherent structures of the 3D data described in Sections III.A and III.B.

The second approach is based on the low-rankness of diffuse reflection components under varying light source directions. Specifically, the image of a Lambertian object under an arbitrary directional light source is represented by the linear combination of three basis images of the object [12][1]. Therefore, we can extract diffuse reflection components from a set of images of an object taken under multidirectional light sources, *i.e.* the slice B in Fig. 2 via low-rank matrix completion and recovery [16] for example.

Unfortunately, however, the approach based on the low-rankness assumes that the light source color is not variable but fixed because the images of an object under multispectral light sources live in 3D subspaces different from each other. Therefore, when it is used independently for each slice with a fixed light source color, we cannot capture the inherent structure of the 3D data under varying light source colors described in Sections III.A. In addition, although the approach based on the low-rankness can extract diffuse reflection components on the Slice B in Fig. 2, there is no guarantee that the remaining components are specular reflection components due to noise.

The third polarization-based approach makes use of the difference of the polarization states of a specular reflection component and a diffuse reflection component. When we observe the reflected light from an object surface illuminated by polarized light, the former is polarized whereas the latter is unpolarized [14]. The polarization-based approach requires a set of images taken by placing linear polarizing filters in front of a light source and a camera, and rotating one of them.

The polarization-based approach is not necessarily suited for multi/hyper-spectral light stages due to the following two reasons. First, placing linear polarizing filters in front of light sources is more burdensome, as the number of light sources increases. Second, more importantly, capturing a large number of images by rotating the linear polarizing filter in front of a camera is time consuming. This is a serious problem for multi/hyper-spectral light stages using LEDs because LEDs are usually dim and require long exposure time.

III. Proposed Method

We assume that the color images of an object of interest are captured from a fixed viewpoint and under multispectral and multidirectional light sources by using a multispectral light stage similar to the existing ones [1], [5], [6] as shown in Fig. 1. Specifically, the light stage has D LED clusters at different directions, and each cluster has C LEDs with different spectral intensities, *i.e.* $C \times D$ LEDs in total.

For the sake of simplicity, we consider the C color images taken under C different light source colors as the $3C$ grayscale images taken under $3C$ different light source colors without loss of generality. We denote the pixel value at the p-th pixel $(p = 1, 2, 3, ..., P)$ under the c-th light source color $(c = 1, 2, 3, ..., 3C)$ and the d-th light source direction $(d = 1, 2, 3, ..., D)$ by i_{pcd}.

A. Varying Light Source Colors and Directions

First, let us consider the slice A in Fig. 2, *i.e.* the variation of pixel values at a fixed pixel but under varying light source colors and directions.

According to the dichromatic reflection model [11], the observed pixel value i_{pcd} is the sum of a specular reflection component and a diffuse reflection component:

$$i_{pcd} = s_{1,c} g_{p1,d} + s_{p2,c} g_{p2,d}, \tag{1}$$

where the first and second terms are the specular and diffuse reflection components respectively. The specular reflection

[1]We mention the effects of attached shadows and/or cast shadows in Section III.B.

component is described by the product of the spectral term $s_{1,c}$ and the geometric term $g_{p1,d}$. The former depends on the spectral intensity of a light source and the spectral sensitivity of a camera, and the latter depends on both the viewing and light source directions. In a similar manner, the diffuse reflection component is described by the product of the spectral term $s_{p2,c}$ and the geometric term $g_{p2,d}$. The former depends on the spectral reflectance of a surface in addition to the spectral intensity and the spectral sensitivity, and the latter depends on the light source direction.

Therefore, the $3C \times D$ matrix $\boldsymbol{I}_p$, whose (c,d)-th element is given by i_{pcd}, is described as

$$\boldsymbol{I}_p = \boldsymbol{s}_1\boldsymbol{g}_{p1}^\top + \boldsymbol{s}_{p2}\boldsymbol{g}_{p2}^\top. \quad (2)$$

Here, the c-th element of the $3C$-dimensional vector $\boldsymbol{s}_1$ is $s_{1,c}$, the d-th element of the D-dimensional vector $\boldsymbol{g}_{p1}$ is $g_{p1,d}$, and so on. The vectors $\boldsymbol{s}_1$ and $\boldsymbol{s}_{p2}$ represent the colors of the specular and diffuse reflection components respectively under varying light source colors. The vectors $\boldsymbol{g}_{p1}$ and $\boldsymbol{g}_{p2}$ represent the intensity profiles of the specular and diffuse reflection components respectively under varying light source directions. It is known that the color of the specular reflection component $\boldsymbol{s}_1$ is the same as the color of the light sources [11], and that the intensity profile of the specular reflection component $\boldsymbol{g}_{p1}$ is sparse since specularity is observed only under a small number of light source directions.

From eq.(2), the matrix $\boldsymbol{I}_p$ is represented as the product of the $3C \times 2$ matrix $\boldsymbol{S}_p$ and the $2 \times D$ matrix $\boldsymbol{G}_p$:

$$\begin{aligned} \boldsymbol{I}_p &= \begin{pmatrix} \boldsymbol{s}_1 & \boldsymbol{s}_{p2} \end{pmatrix} \begin{pmatrix} \boldsymbol{g}_{p1}^\top \\ \boldsymbol{g}_{p2}^\top \end{pmatrix} & (3) \\ &= \boldsymbol{S}_p \boldsymbol{G}_p. & (4) \end{aligned}$$

Thus, the matrix consisting of the pixel values at a fixed pixel but under varying light source colors and directions, *i.e.* $\boldsymbol{I}_p$ has rank 2.

Note that the rank of $\boldsymbol{I}_p$ is 2 even when attached shadows and/or cast shadows are observed at the p-th pixel, because the geometric terms include them. Therefore, we can make use of the rank 2 structure of pixel values on the slice A without paying special attention to those shadows.

B. Varying Pixels and Light Source Directions

Second, let us consider the slice B in Fig. 2, *i.e.* the variation of pixel values under a fixed light source color but at varying pixels and under varying light source directions.

Assuming the Lambert model, the diffuse reflection component, *i.e.* the second term of the right-hand side of eq.(1) is described as

$$s_{p2,c}\,g_{p2,d} = \int l_c(\lambda) r_p(\lambda) s(\lambda) d\lambda \; \boldsymbol{n}_p^\top \boldsymbol{l}_d. \quad (5)$$

Here, $l_c(\lambda)$, $r_p(\lambda)$, $s(\lambda)$, $\boldsymbol{n}_p$, and $\boldsymbol{l}_d$ are the spectral intensity of the c-th light source color, the spectral reflectance at the p-th pixel, the spectral sensitivity of a camera, the surface normal at the p-th pixel, and the d-th light source direction respectively.

Therefore, the $P \times D$ matrix $\boldsymbol{D}_c$, whose (p,d)-th element is given by $s_{p2,c}g_{p2,d}$, is represented as the product of the $P \times 3$ matrix and the $3 \times D$ matrix:

$$\boldsymbol{D}_c = \begin{pmatrix} \vdots \\ \int l_c(\lambda) r_p(\lambda) s(\lambda) d\lambda \; \boldsymbol{n}_p^\top \\ \vdots \end{pmatrix} \begin{pmatrix} \cdots & \boldsymbol{l}_d & \cdots \end{pmatrix}. \quad (6)$$

Thus, the matrix consisting of the diffuse reflection components under a fixed light source color but at varying pixels and under varying light source directions, *i.e.* $\boldsymbol{D}_c$ has rank 3[2]. In other words, the image of a Lambertian object under an arbitrary directional light source is represented by the linear combination of three basis images of the object [12][3].

Note that the rank of $\boldsymbol{D}_c$ deviates from 3 when attached shadows and/or cast shadows are observed under varying light source directions. As described in Section III.D, we remove the effects of those shadows so that we can make use of the rank 3 structure of diffuse reflection components on the slice B.

C. Separating Reflection Components

Based on the structures described in Sections III.A and III.B, we propose a method for separating reflection components in images taken under multispectral and multidirectional light sources as follows:

$$\begin{aligned} \{\hat{\boldsymbol{s}}_{p2}, \hat{\boldsymbol{G}}_p\} = \; & \arg\min_{\{\boldsymbol{s}_{p2}, \boldsymbol{G}_p\}} \frac{1}{2} ||\boldsymbol{I}_p - \boldsymbol{S}_p \boldsymbol{G}_p||_2^2, \; \forall p & (7) \\ \text{subject to} \; & s_{p2,c} \geq 0, g_{p1,d} \geq 0, g_{p2,d} \geq 0, \; \forall p,c,d & (8) \\ & ||\boldsymbol{g}_{p1}||_0 \leq L, \forall p & (9) \\ & \mathrm{rank}(\boldsymbol{D}_c) = 3, \forall c. & (10) \end{aligned}$$

Our proposed method assumes that the color of the specular reflection component $\boldsymbol{s}_1$ is known[4], and estimates the color of the diffuse reflection component $\boldsymbol{s}_{p2}$ and the intensity profiles of the specular and diffuse reflection components $\boldsymbol{G}_p$ for all pixels.

More specifically, based on the rank 2 structure described in Section III.A, our proposed method decomposes the matrix $\boldsymbol{I}_p$ into the matrices $\boldsymbol{S}_p$ and $\boldsymbol{G}_p$ for each pixel as eq.(7). Since both the spectral and geometric terms are non-negative, we impose the non-negativity constraints on the elements of $\boldsymbol{s}_{p2}$ and $\boldsymbol{G}_p$ as eq.(8). In addition, our method takes the sparseness of the intensity profile of the specular reflection component $\boldsymbol{g}_{p1}$ into consideration as eq.(9). Here, L is the parameter for controlling the sparseness. Based on the rank 3 structure described in Section III.B, we impose the rank 3 constraints on the matrix consisting of diffuse reflection components for each light source color as eq.(10).

D. Implementation Details

We solve the optimization problem of eq.(7) with the constraints of eq.(8) to eq.(10) by iteratively using sparse NMF

[2] We assume that an object of interest has 3D shape. Degenerate cases include 1D planar objects and 2D cylindrical objects.

[3] It is clear that those three basis images depend on the light source color as $\int l_c(\lambda) r_p(\lambda) s(\lambda) d\lambda$ in eq.(6). Therefore, the images of an object under multispectral light sources live in 3D subspaces different from each other.

[4] We assume that the spectral intensities of light sources and the spectral sensitivity of a camera are calibrated in advance.

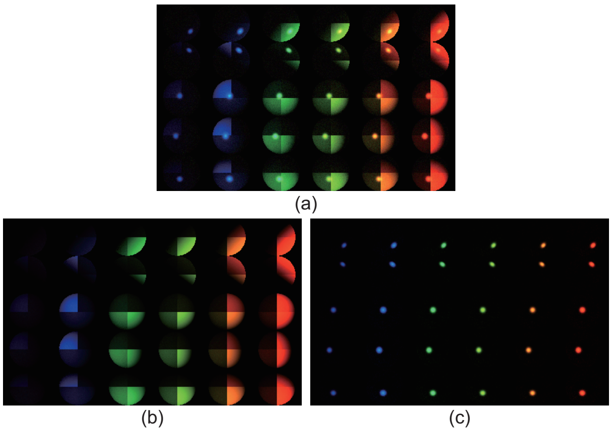

Fig. 3. The results of our proposed method on synthetic images (sphere): (a) the input images, (b) the diffuse and (c) the specular reflection components separated by using our method, when $\sigma = 8$.

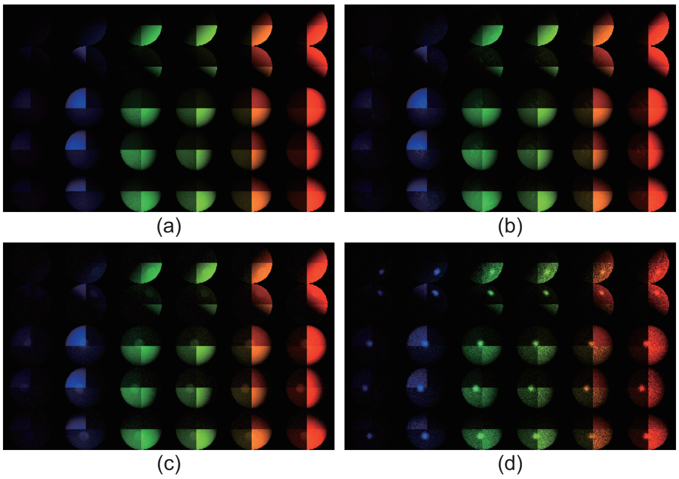

Fig. 4. The comparison with other methods on synthetic images (sphere): the diffuse reflection components separated by using (a) the sparse NMF, (b) the SVD with missing data, (c) Wu *et al.* [16], and (d) Akashi and Okatani [2].

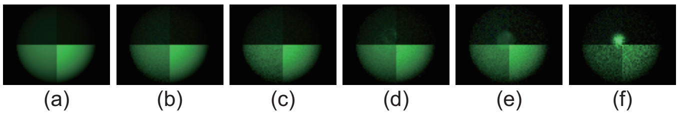

Fig. 5. The diffuse reflection components: (a) the ground truth and those separated by using (b) our proposed method, (c) the sparse NMF, (d) the SVD with missing data, (e) Wu *et al.* [16], and (f) Akashi and Okatani [2]. They are closeups from Fig. 3 and Fig. 4.

(non-negative matrix factorization) on the slice A and SVD (singular value decomposition) with missing data on the slice B in Fig. 2 as follows.

1) For each pixel, updating $\boldsymbol{s}_{p2}$ and $\boldsymbol{G}_p$ by using sparse NMF with L_0 constraints [10].
2) Converting $\boldsymbol{s}_{p2}$ and $\boldsymbol{g}_{p2}$ for all pixels into $\boldsymbol{D}_c$ for all light source colors.
3) For each light source color, approximating $\boldsymbol{D}_c$ with a rank 3 matrix by using SVD with missing data [13].
4) Converting $\boldsymbol{D}_c$ for all light source colors into $\boldsymbol{s}_{p2}\boldsymbol{g}_{p2}^\top$ for all pixels.
5) For each pixel, decomposing $\boldsymbol{s}_{p2}\boldsymbol{g}_{p2}^\top$ into $\boldsymbol{s}_{p2}$ and $\boldsymbol{g}_{p2}$ by using NMF.
6) Repeating 1) to 5) until convergence.

Before the step 1), we compute the median of the $3C$-dimensional pixel colors observed under D light source directions, and use it for initializing $\boldsymbol{s}_{p2}$. In the step 3), we consider shadowed pixels with smaller pixel values than a threshold as missing data. We empirically confirmed that the above optimization is usually converged within a few iterations.

IV. Experiments

To confirm the effectiveness of our proposed method, we conducted a number of experiments by using both synthetic and real images.

A. Synthetic Images

First, we compared the performance of our proposed method with those of the following methods by using synthetic images.

- **Sparse NMF:** This is a building block of our proposed method, in particular eq.(7) to eq.(9), and is based only on the rank 2 structure of pixel values and the sparseness of specular reflection components on the slice A. It has an empirical parameter for controlling the sparseness of specular reflection components.
- **SVD with missing data:** This is another building block of our method, in particular eq.(10), and is based only on the rank 3 structure of diffuse reflection components on the slice B. It has an empirical parameter for removing specular reflection components as outliers by thresholding.
- **Wu *et al.* [16]:** This method makes use of the low-rankness of diffuse reflection components as well as the sparseness of specular reflection components and shadows under varying light source directions[5]. It has an empirical parameter for controlling their sparseness. As described in Section II, we used it for each slice with a fixed light source color.
- **Akashi and Okatani [2]:** This method makes use of the sparseness of body colors in addition to the difference between the colors of a specular reflection component and a diffuse reflection component. It has an empirical parameter for controlling the sparseness of body colors. As described in Section II, we used it for each image.

We synthesized 120 images of a sphere under multispectral and multidirectional light sources. The sphere has texture consisting of 4 different spectral reflectances: the red, green, blue, and yellow from the X-Rite color checker. The number of light source colors is 6 ($C = 6$) and the number of light source directions is 20 ($D = 20$). The spectral intensities and directions of the light sources are the same as those of our multispectral light stage. In order to prevent saturated pixels,

[5] We implemented eq.(9) in their paper by using the augmented Lagrangian multiplier method [7].

TABLE I. THE RMS ERRORS OF THE SEPARATED REFLECTION COMPONENTS: DIFFUSE (TOP) AND SPECULAR (BOTTOM) IN EACH FIELD.

Method\Noise level (σ)	0	1	2	4	8	16
Proposed method	0.11	**0.25**	**0.46**	**0.91**	**1.87**	**4.57**
based on both the structures on the slices A and B	0.11	**0.24**	**0.46**	**0.93**	**1.80**	**3.50**
Sparse NMF	**0.07**	0.32	0.63	1.27	2.51	5.05
based only on the structure on the slice A	**0.11**	0.26	0.48	0.95	1.83	3.54
SVD with missing data	2.74	2.84	3.04	3.63	5.65	13.19
based only on the structure on the slice B	2.19	2.34	2.66	3.57	5.93	11.95
Wu *et al.* [16]	2.27	2.49	2.93	4.12	6.81	12.28
based on low-rankness and sparseness	2.27	2.37	2.52	2.87	3.62	5.11
Akashi and Okatani [2]	18.74	20.37	20.68	21.62	21.77	23.99
based on color and sparseness	18.24	19.79	20.14	21.01	20.83	21.54

we assume HDR images, *i.e.* the pixel values are not 8-bit integers but real numbers. We added Gaussian noise, whose mean and standard deviation are 0 and σ respectively, to each pixel value, and then used them as input. The parameter of our method for controlling the sparseness, *i.e.* L in eq.(9), is empirically set to 5. The parameters of the other methods, one for each method, are tuned so that they perform best.

In Fig. 3, we show some of (a) the input images, (b) the diffuse and (c) the specular reflection components separated by using our proposed method, when $\sigma = 8$. Here, we converted HDR images into 8-bit images for display purpose[6]. We can qualitatively see that our method works well.

In Fig. 4, we show the diffuse reflection components separated by using (a) the sparse NMF, (b) the SVD with missing data, (c) Wu *et al.* [16], and (d) Akashi & Okatani [2] for the comparison with our proposed method. We can see that (a) the result of the sparse NMF is slightly noisier than that of our method. In addition, we can see that some artifacts due to specular reflection components are visible in the results of (b) the SVD with missing data and (c) Wu *et al.* [16]. It is clear that (d) Akashi and Okatani [2] does not work well because the color of a specular reflection component is almost the same as that of a diffuse reflection component due to narrow-band LEDs as suggested also in their paper. The effectiveness of our method is clear from the closeups shown in Fig. 5.

For quantitative comparison, we summarize the RMS (root-mean-square) errors of the separated diffuse and specular reflection components in TABLE I, where σ varies from 0 to 16. We can see that our proposed method works best except for $\sigma = 0$. Specifically, our method based on both the structures on the slices A and B works better than the sparse NMF based only on the structure on the slice A and than the SVD with missing data based only on the structure on the slice B. Therefore, we can conclude that taking all of the inherent structures of the 3D data into consideration is effective for robustly separating diffuse and specular reflection components in images under multispectral and multidirectional light sources. In addition, our method works better than some of the state-of-the-art methods based on low-rankness [16] and color [2].

B. Real Images

Second, we compared the performance of our proposed method with that of the sparse NMF, *i.e.* the second best

[6]The value of σ is defined in 8-bit images and then scaled for HDR images.

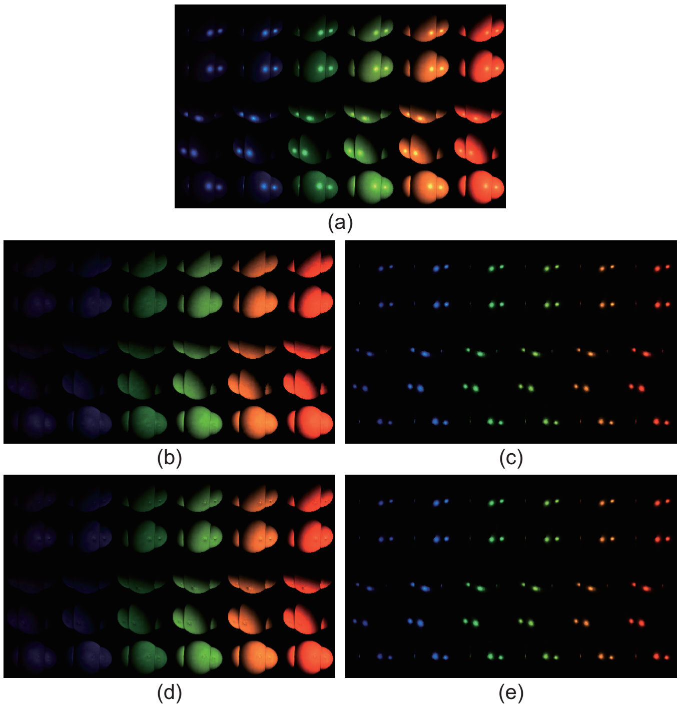

Fig. 6. The results on real images (wooden bread): (a) the input images, (b) the diffuse and (c) the specular reflection components separated by using our method, and (d) the diffuse and (e) the specular reflection components separated by using the sparse NMF.

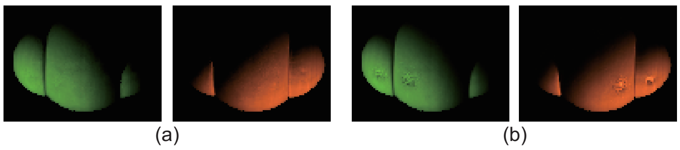

Fig. 7. The diffuse reflection components separated by using (a) our proposed method and (b) the sparse NMF. They are closeups from Fig. 6(b) and (d).

method in TABLE I by using real images. Since it is not easy to acquire the ground truth by using the polarization-based approach as described in Section II, we qualitatively discuss the experimental results.

We used 120 images of target objects captured by using our multispectral light stage termed Kyutech Multispectral Light Stage I [6] in Fig. 1. The number of light source colors is 6 ($C = 6$) and the number of light source directions is 20

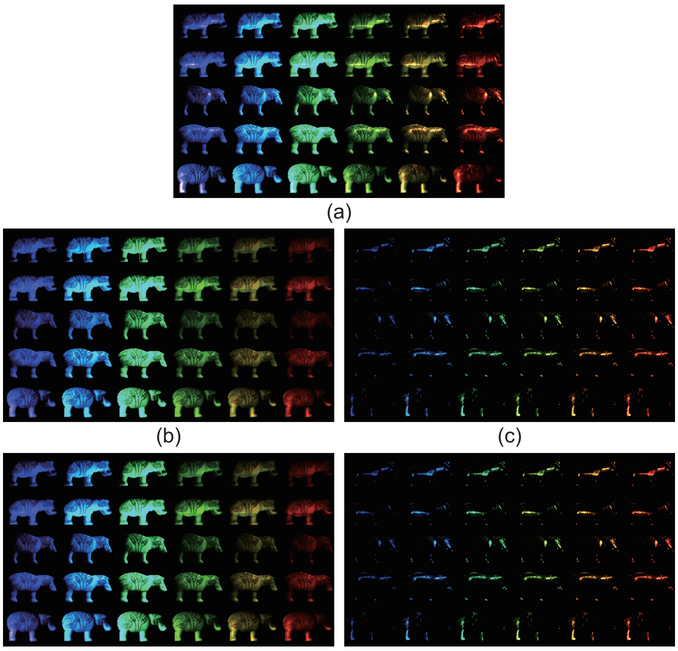

(a) (b) (c) (d) (e)

Fig. 8. The results on real images (ceramic hippopotamus): (a) the input images, (b) the diffuse and (c) the specular reflection components separated by using our method, and (d) the diffuse and (e) the specular reflection components separated by using the sparse NMF.

($D = 20$). The target objects are a wooden bread and a ceramic hippopotamus. We empirically set the parameter L in eq.(9) to 3.

In Fig. 6, we show some of (a) the input images, (b) the diffuse and (c) the specular reflection components separated by using our proposed method, and (d) the diffuse and (e) the specular reflection components separated by using the sparse NMF. We can find that some spot-like artifacts due to specular reflection components are visible in (d) the diffuse reflection components separated by using the sparse NMF. This is because the sparse NMF is applied for each pixel, and does not take the rank 3 structure of diffuse reflection components at varying pixels and under varying light source directions. On the other hand, we can see that (b) the diffuse reflection components separated by using our method is smooth. The effectiveness of our method is clear from the closeups shown in Fig. 7. This result also shows that taking all of the inherent structures of the 3D data into consideration is effective for robustly separating diffuse and specular reflection components in images under multispectral and multidirectional light sources. Fig. 8 shows that our method works well for a different material.

V. Conclusion and Future Work

In this paper, we proposed a robust method for separating diffuse and specular reflection components in a set of images of an object taken under multispectral and multidirectional light sources. Specifically, our proposed method considers the set of images as the 3D data, and then makes use of the inherent structures of the 3D data: the rank 2 structure of pixel values under varying light source colors and directions, the rank 3 structure of diffuse reflection components at varying pixels and under varying light source directions, and the sparseness of specular reflection components. We conducted a number of experiments by using both synthetic and real images, and show that taking all of the inherent structures of the 3D data into consideration is effective for robustly separating reflection components, and that our method works better than some of the state-of-the-art techniques.

The future work of this study includes the extension to other components such as interreflection and fluorescence. The application to computer vision techniques such as photometric stereo, material editing, and relighting is another direction of the future work.

Acknowledgments

This work was supported by JSPS KAKENHI Grant Numbers JP25280057 and JP16H01676.

References

[1] B. Ajdin, M. Finckh, C. Fuchs, J. Hanika, and H. Lensch, "Compressive higher-order sparse and low-rank acquisition with a hyperspectral light stage", Technical Report, Eberhard Karls Universität Tübingen, WSI-2012-01, 2012.

[2] Y. Akashi and T. Okatani, "Separation of reflection components by sparse non-negative matrix factorization", In Proc. ACCV2014, Part V, pp.611–625, 2014.

[3] P. Debevec, A. Wenger, C. Tchou, A. Gardner, J. Waese, and T. Hawkins, "A lighting reproduction approach to live-action compositing", In Proc. ACM SIGGRAPH 2002, pp.547–556, 2002.

[4] M. Fuchs, H. Lensch, V. Blanz, and H.-P. Seidel, "Superresolution reflectance fields: synthesizing images for intermediate light directions", In Proc. EG2007, pp.447–456, 2007.

[5] J. Gu and C. Liu, "Discriminative illumination: per-pixel classification of raw materials based on optimal projections of spectral BRDF", In Proc. IEEE CVPR2012, pp.797–804, 2012.

[6] M. Kitahara, T. Okabe, C. Fuchs, and H. Lensch, "Simultaneous estimation of spectral reflectance and normal from a small number of images", In Proc. VISAPP2015, pp.303–313, 2015.

[7] Z. Lin, M. Chen, L. Wu, and Y. Ma, "The augmented Lagrange multiplier method for exact recovery of corrupted low-rank matrices", UIUC Technical Report UILU-ENG-09-2215, 2009.

[8] C. Liu, G. Yang, and J. Gu, "Learning discriminative illumination and filters for raw material classification with optimal projections of bidirectional texture functions", In Proc. IEEE CVPR2013, pp.1430–1437, 2013.

[9] S. Mallick, T. Zickler, P. Belhumeur, and D. Kriegman, "Specularity removal in images and videos: a PDE approach", In Proc. ECCV2006 Part I, pp.550–563, 2006.

[10] R. Peharz and F. Pernkopf, "Sparse nonnegative matrix factorization with l^0-constraints", Neurocomputing, 80, pp.38–46, 2012.

[11] S. Shafer, "Using color to separate reflection components", Color Research & Application, 10(4), pp.210–218, 1985.

[12] A. Shashua, "On photometric issues in 3D visual recognition from a single 2D image", IJCV, 21(1/2), pp.99–122, 1997.

[13] H.-Y. Shum, K. Ikeuchi, and R. Reddy, "Principal component analysis with missing data and its application to polyhedral object modeling", IEEE Trans. PAMI, 17(9), pp.854–867, 1995.

[14] L. Wolff and T. Boult, "Constraining object features using a polarization reflectance model", IEEE Trans. PAMI, 13(7), pp.635–657, 1991.

[15] R. Woodham, "Photometric method for determining surface orientation from multiple images", Optical Engineering, 19(1), pp.139–144, 1980.

[16] L. Wu, A. Ganesh, B. Shi, Y. Matsushita, Y. Wang, and Y. Ma, "Robust photometric stereo via low-rank matrix completion and recovery", In Proc. ACCV2010, Part III, pp.703–717, 2010.